Regular Article

Microstructure effects on thermal and electrical conductivities in the intermetallic compound Ag₃Sn-based materials, sintered by SPS in view of die-attachment applications

R. Mahayri[1,a] , S. Mercone[1], F. Giovannelli[2], K.-L. Tan[3], J.-M. Morelle[3], N. Jouini[1], and F. Schoenstein[1]

[1] Laboratoire des Sciences des Procédés et des Matériaux (UPR3407), CNRS-USPN, Villetaneuse, France
[2] GREMAN UMR7347 – CNRS, Université de Tours, Parc, Grandmont, TOURS 37200, France
[3] Valeo Equipements Electriques Moteurs SAS, 2 Rue André Boulle, BP 150, 94017 Créteil, France

Abstract Sintered intermetallic Ag₃Sn powders by spark plasma sintering (SPS) have been studied in order to analyse the effect of the microstructure on the transport properties at room temperature. Firstly, we synthesized Ag₃Sn submicronic particles by polyol process. Then, we sintered them by SPS at different temperature (473, 573 and 663 K) and pressure (20 and 100 MPa) using fixed dwelling time of 5 min. X-Ray Diffraction (XRD) and Differential Scanning Calorimetry (DSC) show that all sintered samples remained single-phased according to the Ag₃Sn orthorhombic crystal structure. Their corresponding grain size ($\approx$ 0.65 to 1.75 μ m) and relative density ($\approx$ 88–98%) were calculated and show similar evolution respect to the sintering parameters. As a matter of fact, sintering temperature remains the key factor to affect the microstructure of the sintered material s. Finally, the thermal conductivity and the electrical resistivity were investigated at room temperature by using the Flash Laser technique and the Physical Property Measurement System (PPMS) respectively. The obtained values were highly dependent on densitiy and grain showing the key role of the microstructure and thereby confirming the fact that Ag₃Sn compound is a good candidate for a lead-free die-attach material in power module devices.

1 Introduction

The ongoing research for reliable and environmentally friendly interconnect materials in microelectronics packaging is growing tremendously. This is due to the increasing demand on the development of high power density and high performance power electronics systems. In this frame, Die-bonding materials of high power semiconductor devices must offer high thermal and high electrical conductivities [1], compliance to RoHS directives, lead-free soldering technology [2], low process temperature [3,4], high reliability [5] and the ability to endure high operating temperature (approximately 573 K) [6]. As a matter of facts, Sn–Pb alloys are no longer suitable for such future solders. However, latest works have shown that the intermetallic compound (IMC), Ag₃Sn, can be a good candidate to replace lead-based solders for interconnection in electronic power devices [7,8]. In fact, this compound has a relatively high melting point (480 °C) which offer a thermal stability at different operating and processing temperatures (with a homologous temperature $\approx$ 384 °C), and

at the same time, its electric and thermal properties resemble to those of the eutectic alloy Sn-3.5Ag as well as several lead-free alternatives frequently used in the market [7,8]. We have previously presented the characteristics of Ag₃Sn particles of submicron size, obtained by a soft chemistry polyols process [9,10], that we have been using to sinter the bulk materials reported in this work. The use of submicron particles allows reducing the applied pressure and temperature during sintering [11]. This is mandatory if we aim to use this compound as a Die-bonding material as it allows protecting the power module components from being damaged during processing [12]. Furthermore, the proposed protocol presents an alternative to the sintering process of silver nanoparticles which clearly presents risks of toxicity related to the nanometric character of the particle [13,14]. The synthesized powders have been consolidated by Spark Plasma Sintering. The as-obtained samples have been submitted to thermal and electrical conductivities measurement. The combinations of the various shaping parameters (particularly temperature and pressure) have led to the development of materials with different microstructures (i.e. relative densities, grain size, nature of grain boundaries...). This work constitutes a first step toward the evaluation of the relia-

[a] e-mail: roland.mahayri@lspm.cnrs.fr (corresponding author)

4174

Eur. Phys. J. Spec. Top. (2022) 231:4173–4178

bility of Ag_3Sn as a die-attach for power module. We also report for the first time the microstructure effects on the thermal and electrical conductivities at 300 K of the Ag_3Sn systems. The results have been compared to those of traditional solders.

2 Experimental

2.1 Powder preparation

Powder constituted of Ag_3Sn particles was synthesized by polyol process (Fig. 1) by use of tin (II) chloride ($SnCl_2$, 99%, Honeywell) and silver nitrate ($AgNO_3$, >99%) as metal precursors. Ethylene glycol (EG) (VWR, 98%) is used as a solvent and as a reducing agent for silver ions while sodium borohydride was selected as a reducing agent for tin ions. A surface stabilizer, PVP (Alfa Aesar) was used to prevent particles from coalescing. The precursors were all poured in the Round bottom flask. After synthesis, the powder was subsequently isolated by centrifugation and dried in an oven. More details on the synthesis process can be found in our previous works [9,10].

2.2 Sintering technique

Spark Plasma Sintering (SPS) technique has been used for consolidating the elaborated powders. This technique allows achieving theoretical density of bulk material at lower sintering temperatures compared to conventional sintering techniques. Sintering is realized by a direct current pulse flowing through a mold and by applying a uniaxial pressure at both ends of the mold from above and beneath (Fig. 2). We use graphite molds of 8 and 15 mm in diameter (which allows pressure of 100 and 20 MPa respectively). Once the matrix is filled with the powder, the set is placed between the two electrodes allowing the application of the electric current and the pressure. Heating is then obtained by joule effect under a pulsed current at high intensity and in a high primary vacuum (between 20 and 60 Pa). The SPS used in this work is 'Dr. Sinter LAB Series SPS-515 S'. The mold was loaded with enough powder to obtain a pellet between 2.5 and 3 mm thick by con-

1- Mechanical stirrer

2- Condenser

3- Thermocouple

4- Round-bottom flask (500 ml)

5- Flask heater

6- Thermostat

Fig. 1 Experimental setup of the synthesis of Ag_3Sn particles by polyol process

sidering the density of Ag_3Sn ($9.93\,g/cm^3$) [15] and its lattice parameters. The pulse mode of the SPS system was maintained at the recommended standard 12:2 (on-off, pulse width 3.4 ms). Pressure is varied by changing the applied force and/or by changing the mold diameter. Temperature is controlled by means of thermocouples placed in the matrix near the sample. For every experiment the heating rate was kept at a value of 100 ° C/min. The dwelling temperatures are 473, 573 and 663 K and the applied pressures are 20 MPa and 100 MPa. The dwelling time is fixed to 5 min. All samples and their sintering parameters are shown in Table 1.

2.3 Characterization

Prior to microstructure analysis, polishing steps of the sintered sample were carried out with abrasive papers of 1200, 2400 and 4000 μ m for 5 min each. Then, diamond pastes are used to improve the surface quality (grain size 3 μm and 1 μm during 5 min each). The last step of polishing is done with a 0.25 μm diamond paste for 1 h, followed by the use of colloidal silica (Oxide Polishing Suspensions 'OPS', 200 nm) for the same duration. The nature of the synthesized phases was achieved by x-ray diffraction (XRD) ($20 ° < 2\theta < 120 °$ and $\Delta\,2\theta = 0.03$ °), using Co Kα1 radiation (k = 1.78897 Å) on an INEL Equinox 1000 X-ray diffractometer. XRD characterization was performed by using two software: MATCH was used for the phase identification [16], and MAUD (material analysis using diffraction) [17] was used to perform the Rietveld refinement analysis. In addition, phase identification was carried on by differential thermal analysis (DTA) using Labsys TG-D747 instrument. The morphological observations and the particle/grain size were achieved by scanning electron microscopy (SEM), using a field emission gun scanning electron microscopy (FEG-SEM) model ZEISS^{TM} SUPRA 40 VP. The density of the samples was determined by a pycnometer under inert gas (He) where we use a 10 cm^3 volume cell which is adapted to the dimensions of SPS-samples. The pycnometer model used is AccuPyc II 1340. For thermal conductivity measurement, the SPS-samples were cut and brought to an area of $8 \times 8\,mm^2$ and to a thickness of 2 mm. The thermal conductivity λ is determined by the product of the density $\rho(kg/m^3)$, the thermal diffusivity α (m^2/s) and the specific heat Cp ($J.Kg^{-1}.K^{-1}$) of the sample (equation 1). The thermal diffusivity measurement of all specimens was carried out three times under vacuum at room temperature (Netzsch LFA 457). The heat capacity Cp of the materials was measured from room temperature to 1000 ° C, with a heating rate of 20K·min^{-1} in platinum crucibles in nitrogen atmosphere, using differential scanning calorimetry (STA449F3 Jupiter, Netzsch).

$$\lambda(T) = \alpha(T) \times Cp(T) \times \rho(T) \qquad (1)$$

Electrical resistivity of SPS-samples was measured by PPMS (Physical Properties Measurement System) in the the Van der Pauw configuration (i.e. 4-contacts) after polishing and cutting of the sample (dimensions
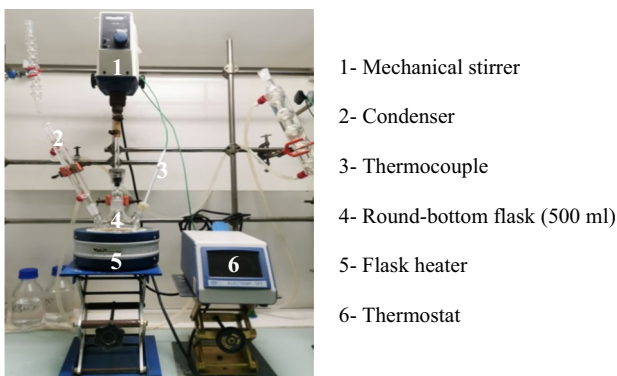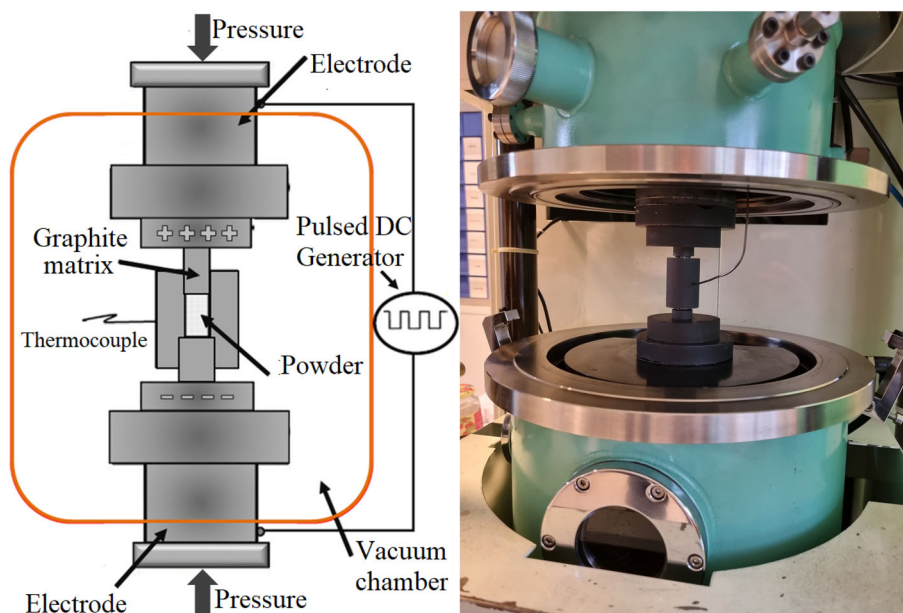
Fig. 2 Scheme of sample positioning in the SPS chamber

Table 1 SPS sintering parameters of Ag_3Sn samples

Sample	Temperature (K)	Pressure (MPa)	Time (min)	Heating rate (° C/min)
Ag_3Sn-1	473	20	5	100
Ag_3Sn-2	573	20	5	
Ag_3Sn-3	573	100	5	
Ag_3Sn-4	663	20	5	
Ag_3Sn-5	663	100	5	

$2 \times 2 \times 10 \, mm^3$). The sample, glued to the sample holder, has been connected by silver wires to the "voltage-current" inlets and outlets of the sample holder. This allows the control by the PPMS of the application and the measurements of the current–voltage (I–V) characteristic and thus the resistivity values.

3 Results

The X-ray diffraction patterns of the synthesized particles and of the SPS-sintered samples are shown in Fig. 3a. All the intense peaks correspond to the orthorhombic Ag_3Sn variety (space group Pmmn). The observed patterns were refined considering the cell parameters and atomic positions of the room temperature (RT) Ag_3Sn variety according to Rossi et al. [18]. The corresponding thermograms (Fig. 3b) confirm the single-phase nature of the compounds by the presence of a unique endothermic peak at around 480 ° C (melting temperature of the Ag_3Sn phase). From X-ray analysis, we notice that the average crystallite size (L) drops drastically after sintering process at 473 K and then increases with the value of the sintering temperature (Table 2). The average size of the crystallites decreases from 623 nm for the powder to 47 nm after sintering process at 473 K, then increases again to 160 and 301 for samples sintered at 573 and 663 K respectively.

SEM analyses were carried out in order to follow the evolution of the nature of the microstructure of the samples with respect to sintering temperatures and pressures. As discussed, an adequate polishing process was optimized in order to improve the quality of the surface and thus of the SEM images. The Ag_3Sn material is relatively a soft compound and thus can easily show wear or usury due to the preparation conditions. SEM micrograph presented in Fig. 4a points out that the Ag_3Sn powder is composed of polydispersed particles in the submicrometer range with some aggregations. The estimated particle size is 0.66 µm which is very close to the average crystallite size (0.623 µm) and reveal that Ag_3Sn particles could probably be formed by Ostwald ripening.

After sintering at 473 K, the grain size is equal to 0.709 µm. For this temperature, the first sintering step is defined by the formation of bridges (and grain boundaries) between the particles followed by the growth of these bridges partially completed in several areas (Fig. 4b). This creates a network of interconnected pores at the end of the sintering. For Ag_3Sn-2 and Ag_3Sn-3 (Fig. 2c, d), sintered at 573 ° K, the sintering process seems to have reached a second stage related to the reduction of the porosity domains. We notice the disappearance/shrinking of these pores over a large area of the sample surface and the creation of individual pores (closed porosity). The average grain size
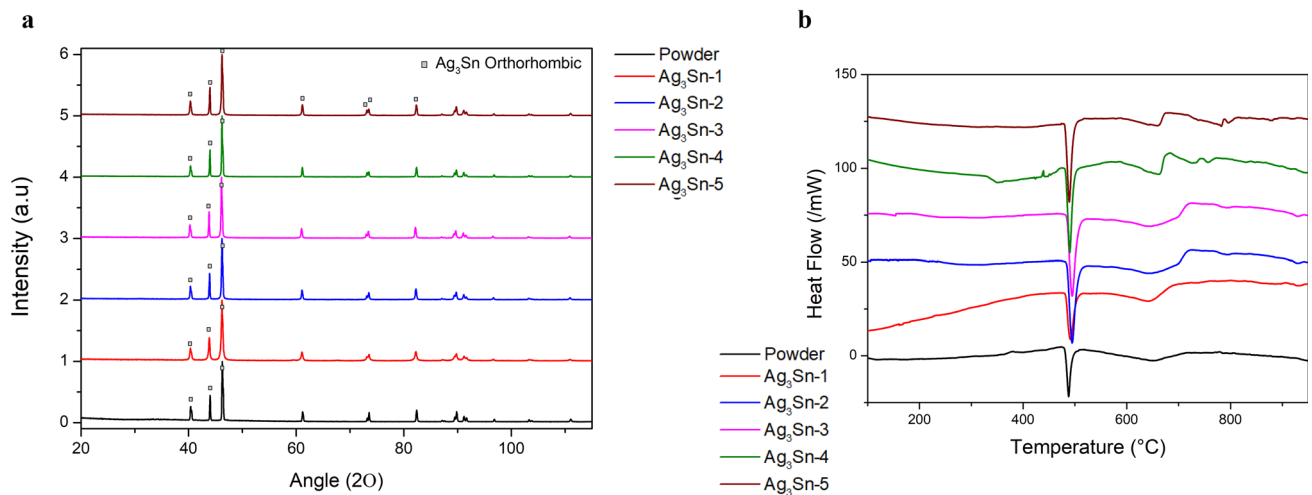
Fig. 3 XRD diagrams (**a**) and thermograms (**b**) of Ag₃Sn powder and SPS-sintered samples

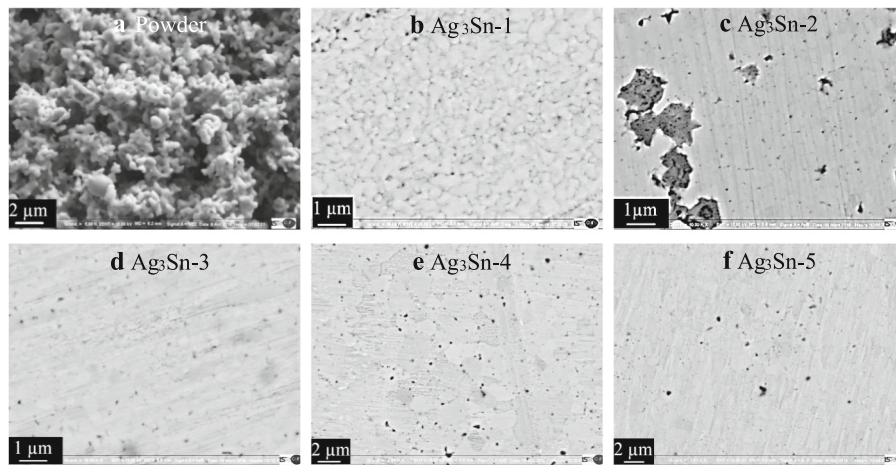**Fig. 4** SEM photos of Ag₃Sn powder and SPS-sintered samples

is slightly larger than that of Ag₃Sn-1 and goes from 0.709 μm to 0.796 up to 0.820 μm. Analysis of the micrographs of the samples sintered at 663 K shows a very sharp decrease in the rate of closed porosity. The increase in the average grain size after the removal (almost total) of the porosities is significant. The average size of these grains, which remained quasi-stable for sintering temperatures less or equal to 573K, increases and goes from around 0.80 μm to 1.73 μm (for Ag₃Sn-4). All values are shown in Table 2.

As mentioned above, the densities of the SPS-samples were measured by a pycnometer. As shown in Table 2, the changes in grain size and relative density as function of the sintering temperature show similar patterns. For both parameters, a slight increase with temperature and pressure is observed when T≤ 573 K. For instance, the grain size is around 0.8 μm when relative density is limited to ≈ 90%, and conversely a sudden increase is observed at 663 K with values around 1.7 μm and 98% respectively.

Finally, in Fig. 3a we report the effect of the microstructure on the evolution of the transport properties of IMC Ag₃Sn at room temperature. As for thermal con-

ductivity (Fig. 5a), it can be clearly seen that density and grain size are the main parameters governing the thermal conductivity values. This latter goes from 16 to 79.2 W.m^{-1}.K^{-1} when relative density increases from 88.6 to 97.8 % and/or grain size from 0.709 to 1.702 μm. The electric resistivity (Fig. 5b) slightly decreased from 2.35 to 1.10 ($\times 10^{-7}$) Ω.m when relative density changed from 88.6 to 89.2 %, and show an important increase up to 10.4 × 10^{-7} Ω.m at higher density (i.e. 97.8%). This demonstrates so far the dramatic effect of the microstructure also in the case of the electric resistivity values (i.e. we observe an increase of one order of magnitude) and thus put in evidence the possibility to control it by tightly controlling the microstructure of the IMC.

4 Discussion

X-ray patterns and DTA thermograms show that SPS-samples kept the single-phased orthorhombic Ag₃Sn variety and that highly dense material can be achieved by our sintering process. The average crystallite size of the powder drops drastically after sintering and

Table 2 Microstructural characteristics of SPS-sintered samples

Sample	Relative Density (%)	Crystallite size L (nm)	Grain size (μ m)	$\sigma_{\mathbf{Grain\ size}}$
Powder		623	0.66	0.02
Ag_3Sn-1	88.6	47	0.709	0.023
Ag_3Sn-2	89.2	160	0.796	0.076
Ag_3Sn-3	90.4	161	0.820	0.050
Ag_3Sn-4	97.9	301	1.728	0.053
Ag_3Sn-5	97.8	221	1.702	0.052
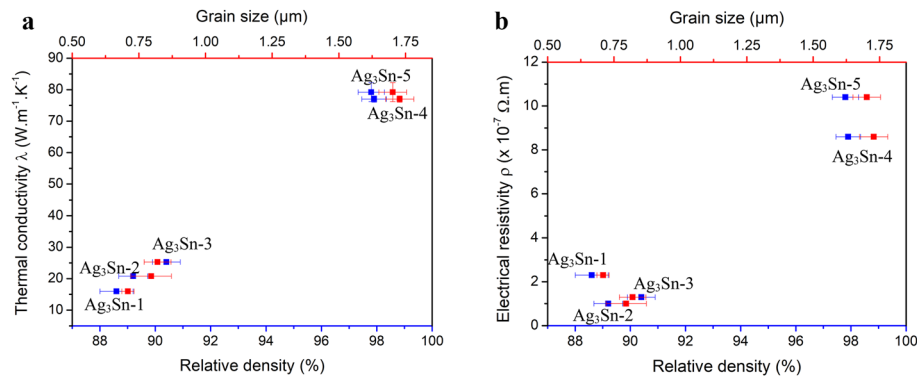
Fig. 5 Thermal conductivity (**a**) and electric resistivity (**b**) at 300 K of SPS-samples as function of relative density and grain size

increases with sintering temperature. This peculiar observation put in evidence that the crystallites may fractionate under the effect of pressure and give rise to the appearance of defects such as intra-granular dislocations. This phenomenon may be thermodynamically compensated when the sintering temperature increases, thus allowing recrystallization of the coherent diffraction domains that lead to their increase in size.

From SEM micrograph in Fig. 2, we calculated the average grain size of each sample and we show that the level of porosity is greatly reduced for high relative density samples ($\approx 98\%$). Results in Fig. 2 Clearly show that the sintering temperature remains the key factor to affect the microstructure of the sintered material. It is interesting to note that as reported earlier [19], the grain size and crystallite size are closely related to each other and increase when the sintering temperature increases. In order to achieve a full densification, it is necessary to cross an "energy barrier" whose temperature is between 573 and 673 K. On the contrary, pressure above 20 MPa does not show any noticeable effect on samples microstructure (see Table 2).

The thermal conductivity measured at 300 K shows that its value linearly increases with the relative density and the grain size underlining again the key role of the microstructure. For high density samples, the values are coherent with the thermal conductivity of bulk Ag_3Sn ($\lambda_{Ag3Sn\,bulk}$ = 76 W.m^{-1}.K^{-1} [20]) and reach 79.2 W.m^{-1}.K^{-1}. We remind here that for power module application, we should take into consideration that a relatively high processing temperature and pressure could damage the chip or other module components. Sintering at 663K or at 100 MPa are not recommended

and do not suit the application in power electronics. If we consider the sample sintered at 573K-20MPa-5min (i.e. low temperature and pressure suitable for applications), the thermal conductivity is equal to 20.8 W.m^{-1}K^{-1},close to that of the solder $Pb_{92.5}Sn_5Ag_{2.5}$ (23 W.m^{-1} K^{-1}) currently used in power modules. Thus, our result shows that although the Ag_3Sn SPS-sample, sintered under suitable conditions for power module applications, is not totally densified, its thermal conductivity is still as good as the one of the commercial solders. Thus it can be considered as a good candidate for the heat transfer delivered by the chip towards the cooling system.

The electric resistivity, also measured at 300 K, has shown two different behaviours. For the first group of samples (Ag_3Sn-1, Ag_3Sn-2) consolidated at a temperature well below the melting point of Ag_3Sn (753 K) and at low pressure (20 MPa), the electrical resistivity decreases when the grain size increases in accordance with the literature [21,22]. It reaches a value of 1.1 $\times$ 10^{-7} Ω.m with grain size of 0.8 μm. This value is close to that of Ag_3Sn bulk (0.8–1$\times$ 10^{-7} Ω.m) [20,23] and smaller than that of $Pb_{92.5}Sn_5Ag_{2.5}$ (2.86$\times$ 10^{-7} Ω.m), $Sn_{63}Pb_{37}$ (1.45$\times$ 10^{-7} Ω.m), Sn-Ag and SAC solders (1–1.5 $\times$ 10^{-7} Ω.m) [24,25].

Conversely, the sample Ag_3Sn-3 consolidated at higher pressure (100 MPa) and the samples Ag_3Sn-4 and Ag_3Sn-5 consolidated at 663 K (i.e. a temperature close to the melting point of Ag_3Sn) show an unexpected behaviour. Their resistivity increases with the grain size. This may be due to the generation of microstructural defects (twins, dislocations, disorder, relative volume of inter-grain boundaries etc) induced

4178

Eur. Phys. J. Spec. Top. (2022) 231:4173–4178

by the higher pressure applied in the first sample (100 MPa) and by the rapid cooling from a state close to the liquid one for the last two ones. Furthermore, the influence of these defects on the scattering of electrons can be reinforced by the relatively high thermal agitation at the measurement temperature (300 K). Similar results have been reported by Kardashev et al. in the case of Ti alloys elaborated by Severe Plastic Deformation (SPD). Indeed these authors have shown that electrical resistivity does not depend on the grain size but on the relative volume of inter-grain boundaries and their particular state [26].

Further work is in progress to understand the observed behaviour: study of electrical resistivity as function of temperature, careful High resolution TEM observations.

5 Conclusion

In conclusion, we consolidated the intermetallic Ag_3Sn powder by spark plasma sintering in order to study the effect of microstructure on the transport properties at room temperature. Our results show that the electric and thermal conductivities highly depend on the microstructure of the sintered samples. We demonstrate that controlling the microstructure of the IMC, based on sintered Ag_3Sn powder, allows the tuning of the conductivities for further applications in power module. So far, we have shown that transport values remain close to those of traditional solders used in technological applications. Due to its low melting temperature and good transport properties, Ag_3Sn appears as a promising die-attach material for semiconductor power devices.

References

1. G. Bai, *Low temperature Sintering of Nanoscale Silver Paste for Semiconductor Device Interconnection* (Ph.D. dissertation, Virginia Polytechnic Institute and State University, Blacksburg, Virginia, Oct) (2005)
2. Directive 2011/65/EU of the european parliament and of the council on restriction of the use of certain hazardous substances in electrical and electronic equipment (recast) (European Union, n ° 165) (2011)
3. T. Lindhqvist, R. Lifset, J. Ind. Ecol. **7**, 3 (2008)
4. T. Wang, X. Chen, G-Q. Lu and G.-Y. Lei, J. Electron. Mater., vol.36, n ° **10**, 1333–1340 (2007)
5. M. Knoerr, A. Schletz, Power Semiconductor Joining through sintering of Silver Nanoparticles: Evaluation of Influence of Parameters Time, Temperature and Pressure on Density, Strength and Reliability. Integrated Power Systems (CIPS), Nuremberg, Germany, mar, V. Verlag, Ed., no. 10.3 (2010)
6. G. Miller, New Semiconductor Technologies Challenge Package and System Setup. 6th International Conference on Integrated Power Electronics System; Nuremberg, Germany, p. 1 (2010)
7. V.R. Manikam, K.Y. Cheong, IEEE Trans. Compon. Packag. Manuf. Technol. **1**, 457 (2011)
8. K. Suganuma, S.J. Kim, K.S. Kim, JOM **61**, 64 (2009)
9. F. Schoenstein, N. Jouini, P. Canaud, J.-M. Morelle, K.-L. Tan, F. Maroteaux, Formulation d'un composé intermétallique Ag-Sn (Patent n ° FR1661461. 24 November) (2016)
10. P. Canaud, R. Mahayri, F. Schoenstein, E. Gautron, K. L. Tan, T. Chauveau, J. M. Morelle, F. Maroteaux, N. Jouini, J. Electron. Mater., vol. 48, n ° 17 (2019)
11. K.S. Siow, J. Alloys Compd. **514**, 6–19 (2012)
12. F. L. Henaff, *Contribution à l'étude, la mise en oeuvre et à l'évaluation d'une solution de report de puce de puissance par procédé de frittage de pâte d'argent à haute pression et basse température* (Ph.D. dissertation, Université de Bordeaux, Bordeaux, France). (2014) (Available on https://tel.archives-ouvertes.fr/tel-01198670/document)
13. M. Reyner, Nanomaterials: Current situation and prospects in occupational health and safety. INRS, Hyg. Sec. Trav, n ° 232 (2013)
14. A. Elsaesser, C.V. Howard, Adv. Drug Deliv. Rev. **64**, 129–137 (2012)
15. E. Ronnebro, J. Yin, A. Kitano, M. Wada, T. Sakai, Solid State Ion. **176**, 2749–2757 (2005)
16. http://www.crystalimpact.com/match/
17. F.L. Lutterotti, M. Bortolotti, G. Ischia, I. Lonardelli, H.R. Wenk, Z. Kristallogr, Suppl. **26**, 125 (2007)
18. P.J. Rossi, N. Zotov, E.J. Mittemeijer, Z. Kristallogr. **231**, 1 (2016)
19. M. A. Bousnina, F. Schoenstein, S. Mercone, N. Jouini, Metals, vol. 10, n ° 112 (2020)
20. A. Lis, high power electronics packaging by transient liquid phase bonding (Ph.D. dissertation, ETH zurich) (2015)
21. O. Ivanov, O. Maradudina, R. Lyubushkin, Mater. Char. **99**, 175–179 (2015)
22. M. Kawamura, R. Sagara, Y. Abe, T. Kiba, K. Ho Kim, Jpn. J. Appl. Phys., vol. 59, n ° 048001 (2020)
23. Y. Tian, Q. M. Zhang, Z. Q. LI, Solid State Commun., n ° 151, pp. 1496–1499 (2011)
24. M. Barrière, *Assemblages de puissance innovants haute température – haute tension pour composants Si dédiés aux applications embarquées aéronautiques, automobiles et ferroviaires* (Ph.D. dissertation, University of Bordeaux). (2017) (Available on https://tel.archives-ouvertes.fr/tel-02388495/document)
25. https://www.ametek-coining.com/knowledge/data-sheet-library/technical-data-sheets
26. B. K. Kardashev, K. V. Sapozhnikov, V. I. Betekhtin, A. G. Kadomtsev, M. V. Narykova, Solid State Phys., vol. 59, n ° 12, pp. 2381–2386 (2017)